J. Indian Soc. Coastal Agric. Res. 40(2): 14-32 (2022) https://doi.org/10.54894/JISCAR.40.2.2022.125302

An Innovative Approach to Delineate and Differentiate Clear and Turbid Water Ponds in Indian Sundarban Area Using Sentinel-2 MSI Data

N. SUDARSAN[1], TANUMI KUMAR[2], CHALANTIKA LAHA SALUI[1], K. CHANDRASEKAR[3] and SOUMYA BANDYOPADHYAY[2]

[1]Indian Institute of Engineering Science and Technology, Shibpur, Howrah - 711 103, West Bengal, India
[2]Regional Remote Sensing Centre - East, NRSC, ISRO, New Town, Kolkata - 700 156, West Bengal, India
[3]National Remote Sensing Centre, ISRO, Hyderabad - 500 037, Telangana, India

Received: 30.06.2022 Accepted: 29.12.2022

Pond water is the main source of irrigation in the Sundarbans area of West Bengal. The serious issues faced in agricultural lands and ponds are due to salinity. As salinity cannot be detected on high scales through satellite images, in this study the remotely sensed turbidity has been compared and studied with laboratory-measured salinity. The high-resolution Sentinel-2 MSI data with optimum bands for water quality detection have been used in this study. The small agricultural ponds in the study area were not detected by the conventionally used water indices, as the ponds were surrounded by homestead vegetation. Hence, a new index called Pond Probability Spectral Index (PPSI) was formulated and used in the decision tree algorithm to delineate all the ponds. Turbidity indices were used over the extracted ponds to classify them into three classes, clear, turbid and highly turbid. From the field accuracy assessment, one of the turbidity indices out performed in segregating the ponds with an overall accuracy of 83.3%. It was also found that salinity was inversely proportional to turbidity only when the turbidity value was greater than 100 NTU. The total estimated pond area (average of 3 seasons) in the Sundarban region was 471.66 km^2.

(***Key words:*** *Decision tree, Remote sensing, Salinity, Sundarbans, Turbidity index, Water quality)*

Water is the most essential resource for mankind's survival. Mostly in tropical regions, drinking, industrial and agricultural needs depend on the inland surface waters. In the last few decades awareness of environmental pollution has increased exceedingly. The consequence of water stress has decreased the allocation of freshwater to agriculture. This phenomenon is expected to continue and intensify in less developed areas, that already have high population growth rates and suffer from serious environmental problems. Due to the increase in stressors such as climate change, anthropogenic influence and eutrophication, monitoring of water quality is gaining importance (Dörnhöfer *et al.,* 2016).

The capillary rise of saline water affects the agricultural ponds and bheries in the Sundarbans area of West Bengal. There is a paucity of research in the remote sensing of surface water salinity (Li-Gang *et al.,* 2008), so in this study, optically active constituents like turbidity have been detected and the goal was to formulate a relationship between turbidity and salinity to bridge the gap.

Turbidity is the main water quality parameter and an important indicator of water degradation (Petus *et al.,* 2010). Turbidity can also be defined as the "cloudiness" or "haziness" present in the water. There are several causes of turbidity; turbidity may be due to the presence of dissolved matter and suspended solids, such as dyes, microscopic organisms, coloured dissolved organic matter (CDOM) or commonly occurring clay and silt.

In the mega-delta coastal areas of Vietnam, Bangladesh and India, surface water is most susceptible to degradation by seawater intrusion, endangering more than 25 million people at risk of using saline water for their daily needs. Moreover, increased salinity and flow in streams and wetlands are likely to make an issue of the

**Corresponding author:* E-mail: sudarsan3010@gmail.com

salt tolerance of vegetation resulting in the reduction of plant growth. Many plants can tolerate higher salinities for shorter periods but cannot survive long periods of inundation.

Geospatial technology is the only optimum way for providing spatial coverage at scales ranging from the regional to the global level. Optical sensors of new generations, such as Sentinel-2 and Landsat-8, present a scientific opportunity for inland water research (Martins *et al.,* 2017; Palmer *et al.,* 2015). But the multispectral imager (MSI) on-board Sentinel-2A delivers images with high spatial (10-30 m), temporal (5 days) and radiometric (12 bits) resolutions (Martins *et al.,* 2017). These high-resolution data are useful in the mapping of small and erratic surface waters, bio-optical parameters of water and water composition changes with greater sensitivity (Du *et al.,* 2016). Many researchers have proved that Sentinel-2 MSI data is the best to study the optically active components of water such as chlorophyll-a (Chl-a), turbidity and CDOM (Dörnhöfer *et al.,* 2016; Martins *et al.,* 2017).

Optically active components in the water bodies qualitatively and quantitatively influence the nature of the spectral signatures. Only the visible part of electromagnetic radiation can potentially provide us with information about the water constituents, as water itself absorbs light strongly at higher wavelengths (Kutser *et al.,* 2016). The clear water has a comparatively higher reflectance in the green band than that of the red band, and the turbid water behaves like bare soils, *i.e.*, the red band reflectance is more than the green reflectance. Various researchers have proved that turbidity in the surface water can be detected from the spectral change in green and red bands (Somvanshi *et al.,* 2012; Quang *et al.,* 2017). A normalised difference index for turbidity (NDTI) has been formulated by Lacaux *et al.* (2007) and found successful over the ponds of Senegal. Later, Elhag *et al.* (2019) used NDTI over the Dam/Lake for turbidity retrieval. Still, now no studies have been carried out in the Sundarbans area for turbidity detection in ponds. So, this index has been applied over our study region and checked for the reliability of the index through field validation. In the present study, this normalized index has been mathematically modified to enhance the values and the accuracy of both indices was compared.

The objectives of the present work were: (i) to develop an algorithm to segregate all small agricultural ponds and bheries from the study area, (ii) to formulate an index/indices to detect turbidity from remotely sensed data and elucidate the spatial and temporal variation of turbidity concentrations and (iii) to find the relationship of turbid ponds with saline ponds using in-situ measurements.

MATERIALS AND METHODS

Study area

Sundarbans lies in the Ganges delta which is the world's largest delta and occupies the lower part of the Bengal Basin of the South Asian region of Bengal. The potential zone extends between 21°32′ and 22°40′ N latitude and between 88°05′ to 89°00′ E longitude, and the region is demarcated by the river Hooghly on the west, the Bay of Bengal on the south, the Ichamati-Kalindi-Raimongal rivers on the east and the Dampier-Hodges line on the north (Ghosh, 2017). Sixty per cent of the total Sundarbans lies in Bangladesh, while the remaining 40% constitute the Indian Sundarbans. The land area measures about 9629 km^2, of which, 4493 km^2 is inhabited by humans and the rest is a reserve forest.

The Indian Sundarbans is distributed across two southern most districts of West Bengal, namely North 24 Parganas and South 24 Parganas (Fig.1). It comprises nineteen blocks, namely, Haroa, Hasnabad, Hingalganj, Minakhan, Sandeshkhali-I and Sandeshkhali-II in North 24 Parganas district and Basanti, Canning-I, Canning-II, Gosaba, Joynagar-I, Joynagar-II, Kakdwip, Kultali, Mathurapur-I, Mathurapur-II, Namkhana, Patharpratima and Sagar in South 24 Parganas District. There are 54 islands in this region.

Datasets used

For the present study, three seasons were considered, winter, summer and post-monsoon and for the reliability of the data validation winter season have been chosen at first. Initially, the winter 2018 dataset have been used as a training dataset for formulating the algorithm. Later, the formulated algorithm was applied to the winter 2019 dataset, which was later validated through field data. The successful algorithm has been applied to the post-monsoon and summer datasets to study the variations within the seasons. So, three-season data of Sentinel-2

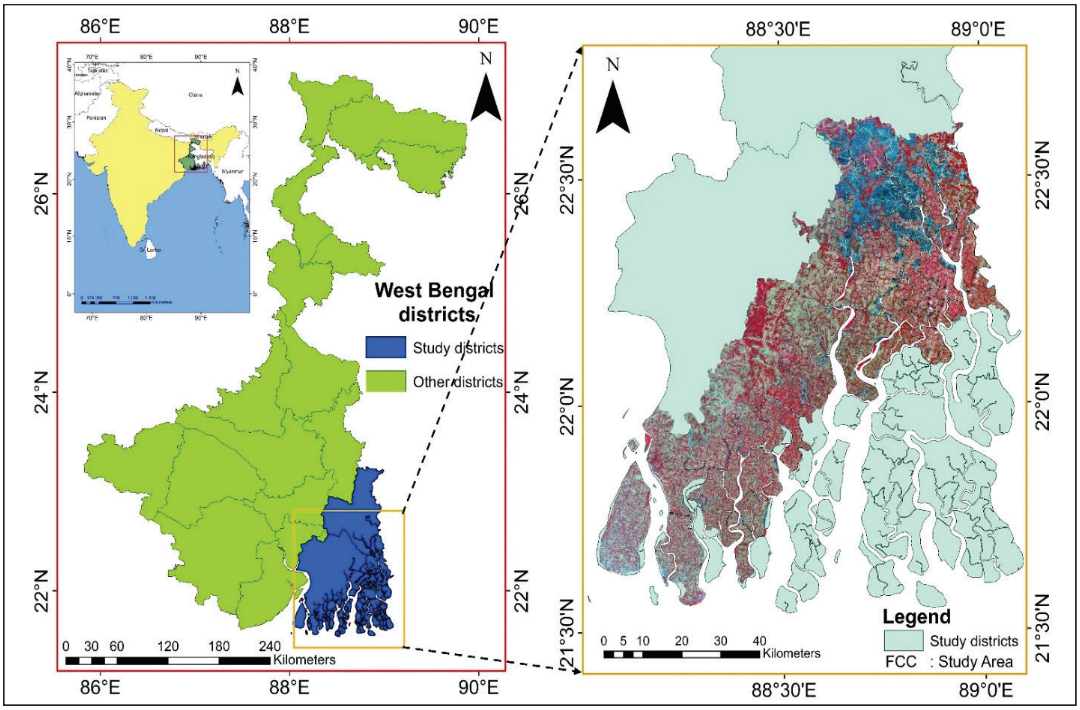

Fig. 1. *Map of the study area*

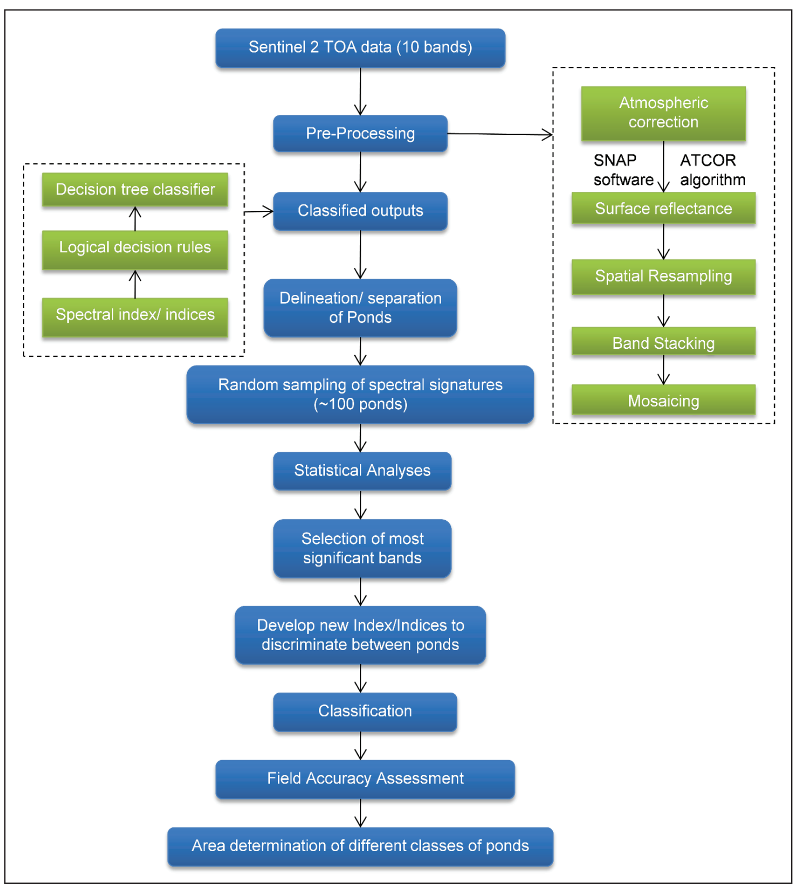

Fig. 2. *Methodology flow chart of the present study*

Table 1. *Sentinel-2 MSI datasets used in the study*

Sl. No.	Season	Date of Sensing (mm/dd/yyyy)	Tiles
1	Winter 2018-19	01/05/2019	R033-QXE,QXD,QYE,QXF
2	Winter 2017-18	12/01/2017	R033-QXE,QXD,QYE,QXF
3	Post Monsoon 2017	10/17/2017	R033-QXE,QXD,QYE,QXF
4	Post Monsoon 2018	10/22/2018	R033-QXE,QXD,QYE,QXF
5	Summer 2018	04/15/2018	R033-QXE,QXD,QYE,QXF
6	Summer 2019	03/26/2019	R033-QXE,QXD,QYE,QXF

were downloaded for 2 years (6 datasets) (Table 1). The brief methodology flow chart has been shown in Fig. 2.

Atmospheric correction

It is necessary to measure the water leaving reflectance (that is surface reflectance) to deal with the water quality parameters (Kutser *et al.,* 2016; Toming *et al.,* 2016). Hence the image has been atmospherically corrected using the Sen2Cor algorithm in SNAP software. Sen2Cor uses the aerosol (443 nm), water vapour (945 nm) and cirrus bands (1375 nm) (band numbers 1, 9 and 10) to convert from the top of atmospheric (TOA) reflectance to bottom of atmospheric (BOA). The Sentinel-2A format, was not directly available at the time of work so the 1C format was downloaded and the atmospheric effect was removed. After processing the data in the Sen2Cor the Sentinel-2 image changes from 1C to 2A format. Due to the coarse spatial resolution of bands 1, 9 and 10, these have not been used further in the study. The atmospherically corrected bands of 20 m resolution were brought down to 10-meter spatial resolution to match with the other four bands by using the nearest neighbour resampling technique in ENVI 5.3.

Extraction of ponds

Many authors have used different classification techniques like supervised and unsupervised methods (Rana and Neeru, 2017), support vector machine (Sarp and Ozcelik, 2017), and object-oriented method (Jawak *et al.,* 2015) to delineate water bodies. But, in the current study area, all the agricultural ponds do not have pure reflectance of water. Due to the mixture of pixel values of vegetation and ponds, very small agricultural ponds (400 m^2) which were surrounded by home-stead vegetation could not be detected by the conventional water detection indices or supervised classification techniques. Hence, spectral correlation fitting, a kind of spectral matching algorithm could be effectively used to determine the resemblance between spectra by computing their correlation coefficients.

In the present study, the ponds were divided into two types, based on their spectral profile *i.e.*, Type 1 ponds which are ponds having the typical spectral signature of water, and Type 2 ponds that visually appear as ponds in false colour composite (FCC) image but does not have the spectral signature of water. The spectra of both ponds were collected and used as training data. A decision tree (DT) classifier powered with a co-relation algorithm (Pearson correlation) has been used to detect those ponds. Many studies have been done where the decision tree was used to extract waterbodies or to differentiate between the waterbodies (Lacaux *et al.,* 2007; Müller *et al.,* 2019).

Pearson correlation coefficient establishes a correlative measure parameter which gives the level of intensity of relationships between the variables. For example, Kumar *et al.* (2017) adopted this method for mangrove classification in the same Sundarbans area and found it to be successful and Hendges *et al.* (2018) used Pearson correlation for correlating the temperature over the water bodies with the average temperature of that class. Recently, Shah and Zaveri (2021) used Pearson's correlation coefficient-based convex geometry for end member extraction from a hyperspectral image. According to the authors' knowledge, this is the first work where the correlation formula has been used in the detection of different types of waterbodies from the same dataset and later combined by using the decision tree classifier.

For the detection of all agricultural ponds from the study area, a decision tree (DT) classifier has been used. The Pearson correlation formula has been named pond probability spectral index (PPSI) further in the study. The ponds present in the study area were divided into two, one with the pure reflectance of water and the other without the reflectance of typical water (mixed pixels), *viz.*, Type 1 ponds and Type 2 ponds, respectively.

The statistical significance of the bands to classify the ponds into two were checked by one-way ANOVA. The results (Fig. 3) revealed that the differences in the mean reflectance values between the two types of spectra were statistically significant. Thus, all 10 bands have been used for the extraction of water bodies. The pure spectra of Type 1 ponds and Type 2 ponds were collected separately and used in $PPSI_1$ and $PPSI_2$ respectively, as training spectra. Consecutively, the results of $PPSI_1$ and $PPSI_2$ were combined by using the decision tree classifier along with the NDVI filter which was used to eliminate the vegetation bunds detected along with Type 1 ponds.

The mean spectral reflectance values of the training data of each band have been substituted in 'b_i' (in Eq.1) and the corresponding band's reflectance valuehas been substituted in 'B_i' (in Eq.1). Hence the resultant $PPSI_{(1, 2)}$ image will have the values from -1 to +1 showing the intensity of correlation with the reference spectrum. This was executed separately for Type 1 and Type 2 ponds with two different training data. The PPSI was

One way ANOVA results

Wavelength (nm)	*F* value	*P* value
490	397.551	0.000
560	612.972	0.000
665	451.277	0.000
705	245.194	0.000
740	5.855	0.003
783	4.525	0.011
842	10.408	0.000
865	12.645	0.000
1610	66.836	0.000
2190	40.033	0.000

Post Hoc results

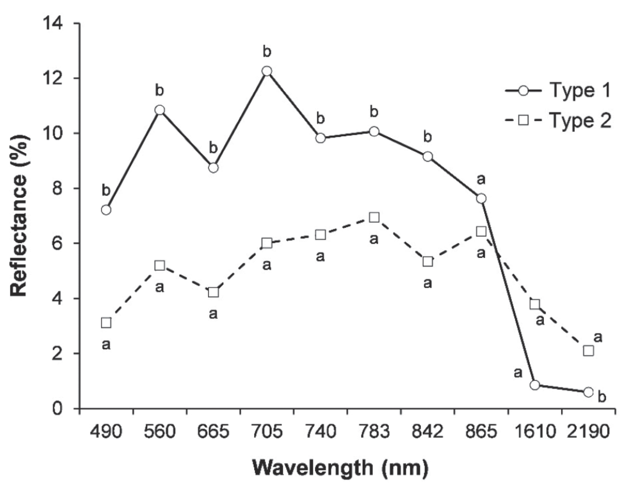

Fig. 3. *ANOVA test results and Post Hoc results showing the consistency between of the bands to differentiate into Type 1 & Type 2 ponds*

calculated using the band math tool in ENVI 5.3 as follows:

$$PPSI(1,2) = \frac{n\sum_{i=1}^{n} B_i b_i - \sum_{i=1}^{n} B_i \sum_{i=1}^{n} b_i}{\sqrt{n\sum_{i=1}^{n} B_i^2 - (\sum_{i=1}^{n} B_i)^2}\sqrt{n\sum_{i=1}^{n} b_i^2 - (\sum_{i=1}^{n} b_i)^2}} \quad \ldots (1)$$

Where,

n = total number of bands in the image (10 in the present study),

B_i = reflectance value at band i for a pixel of the reflectance image and

b_i = reflectance value at band i for a reference spectrum of ponds.

Development of turbidity index

To select the most optimal bands for quantitative analysis of spectral separability, stepwise discriminant analysis (SDA) was performed (Zhang *et al.*, 2014). SDA is one of the most efficient statistical techniques used to discriminate between groups, forward linear SDA has been used in this work. At each step, all variables are evaluated within the model. Those variables that fail to meet the set criterion to stay within the model are removed stepwise, whereas those that can contribute most to the discriminant function are retained within the model based on the F value and Wilks' lambda (L). The procedure stops when no further variables are removed (Zhang *et al.*, 2014). Higher discrimination between the bands is seen when high F and low L values are combined, and an L value of 0 indicates full separability. Alinear combination of the four most significant and uncorrelated bands was obtained from SDA (Table 2).Based on SDA results, four bands (560nm, 705nm, 490nm and 665nm) were found to be most significant in differentiating between the ponds and hence were selected for formulating turbidity indices.

The best-performing index was applied to the extracted ponds from the remaining five study datasets. The total surface area of ponds was calculated for the three seasons. Moreover, season-wise area statistics were computed for all the turbidity classes. In addition to the total pond area season-wise pond areas under the different turbidity classes for each of the 19 blocks were calculated.

Normalized difference turbidity index (NDTI)

Normalized difference turbidity index (NDTI) (Eq. 2) was coined and used by (Lacaux *et al.,* 2007). Several researchers have used this index for segregating turbid ponds (Elhag *et al.,* 2019; Somvanshi *et al.,* 2012; Quang *et al.,* 2017). This conventional index was used to differentiate ponds from the dataset and was used later to compare the accuracy with the new index.

$$\text{Normalised Difference Turbidity Index (NDTI)} = \frac{R(665) - R(560)}{R(665) + R(560)} \quad \ldots (2)$$

where,

R( ) = Reflectance of a band at the central wavelength

Squared normalised difference turbidity index (SNDTI)

In the present work, NDTI was modified by squaring the reflectance values of the green and red bands in equation 3. This was done to enhance the values of the index, which results in a more easy and accurate determination of the absolute threshold. Increasing, the powers to 3, 4, etc., may enhance the values more and more, but by the trial-and-error method, the power raised to 2, excelled the performance in determining the threshold (Table 3). This modified index was named as squared normalised difference turbidity index (SNDTI).

Table 2. *Stepwise discriminant analysis (SDA) results of training pond spectra collected from winter 2019 dataset*

Step	Wavelength in nm	*L*	*F* value
1	560	0.015	550.267
2	560, 705	0.010	244.843
3	560, 705, 490	0.000	161.017
4	560, 705, 490, 665	0.000	127.229

$$\text{Squared Normalised Difference Turbidity Index} = \frac{(R(665))^2 - (R(560))^2}{(R(665))^2 + (R(560))^2} \quad \ldots..(3)$$

where,

R( ) = Reflectance of a band at the central wavelength

Field data and accuracy assessment

Field sample collections were carried out in the first week of January to actively match the sensing date of the winter 2019 dataset. In total, 71 ponds were selected which spread across the study area and effective sampling was done (Fig. 4). The water samples from ponds were collected in acid-washed LDPE (low-density polyethylene) Tarson bottles and were taken for the laboratory and tested for the parameters like turbidity and salinity.

The testing of turbidity has been done according to IS3025 (part 10), 1984, and Eutech instrument TN-100 was used to measure turbidity, which has the range of 0 to 1000 NTU. Based on the various literature studied (Asrafuzzaman *et al.,* 2011; Al-Sameraiy, 2012; Somvanshi *et al.,* 2012) and with the laboratory results, in the present study the turbidity of the ponds could be classified into three classes, *viz.*, clear [0 to 50 nephelometric turbidity unit (NTU)], turbid (50 to 150 NTU) and highly turbid (>150 NTU). These threshold ranges formed were already used in that particular geographical area and found successful by Mukherjee (2014).

All the samples were measured together and the laboratory result of 35 samples has been used to determine the threshold in the output images of NDTI and SNDTI to divide the values into 3 classes (Clear, turbid and highly turbid). The remaining 36 samples have been used as validation data. The turbidity value of all 36 ponds have been taken as point data and overlayed over the NDTI and SNDTI and their respective class values have been appended to the attribute table using 'extract multi value to points' command in ArcGIS. Later, this has been used for overall accuracy assessment and kappa co-efficient determination by the confusion matrix method.

The electrical conductivity (EC) was measured by using the conventional two-probe EC meter. The EC values were in µS cm^{-1} and later it was converted to salinity in parts per thousand (ppt) by an empirical relation (Eq. 4) (Krishan *et al.,* 2021; Rusydi, 2018).

Salinity = 0.67 x Electrical conductivity…(4)

The salinity value of 2 ppt has been considered as the threshold value (IS10500:2012), a salinity value less than 2 ppt has been considered as fresh and greater than 2 ppt has been considered as saline. The result of all 71 samples has been used to develop a relationship between turbidity and salinity.

RESULTS AND DISCUSSION

Delineation of ponds

The PPSI outputs of Type 1 and Type 2 ponds are represented in Fig. 5a and b, respectively. The use of two PPSI has been justified by mapping the same geographical extent of Type 1 and Type 2 outputs (Fig. 6b). From Fig. 6b, it is observed that the small ponds which were detected in Type 2 output were not detected in Type 1 output.

Table 3. *Examples of numerical substitution to represent the enhancement of the values in SNDTI in comparison to NDTI*

Condition	R(665)	R(560)	NDTI (Eq. 3)	SNDTI (Eq. 4)
R (665) = Max, R (560) = Min	0.9	0.1	0.80	0.98
R (665) > R (560)	0.6	0.3	0.33	0.60
R (665) < R (560)	0.4	0.5	-0.11	-0.22
R (665) = Min, R (560) = Max	0.1	0.9	-0.80	-0.98

R() = Reflectance of a band at central wavelength; Max – maximum; Min – minimum; NDTI – Normalised Difference Turbidity Index; SNDTI – Squared Normalised Difference Turbidity Index

Even though the two PPSI outputs at the threshold detected all ponds in the region, the data has been integrated into a single dataset using the decision tree (DT) classifier along with the NDVI threshold applied over the Type 1 output. Thus, the final DT was made by combining the PPSI Type 1 with NDVI threshold and Type 2 outputs (Fig. 6a). The pixel values of PPSI Type 1 varied from - 0.88 to 0.99 with an average of 0.05 and for the PPSI Type 2 varied from - 0.64 to 0.99 with an average of 0.18. The values in the NDVI ranged from -1 to 1. The different thresholds applied for the PPSI Type 1, Type 2 and NDVI are denoted in Fig. 6a. Same geographical extent of the two outputs was compared together (Fig. 6) to illustrate the difference of using NDVI in decision tree classification. The output dataset without using NDVI in the DT and after applying NDVI was compared together in Fig. 6c. From that it has been demonstrated that the vegetation bunds around the water body were removed after applying the NDVI threshold. Lacaux *et al.* (2007) used NDVI thresholding in the decision tree to distinguish ponds with and without vegetation. Similarly, the reverse technique was successfully used in our study through a decision tree to remove the vegetation bunds by using the NDVI threshold and also to combine both outputs of Type 1 and Type 2 ponds.

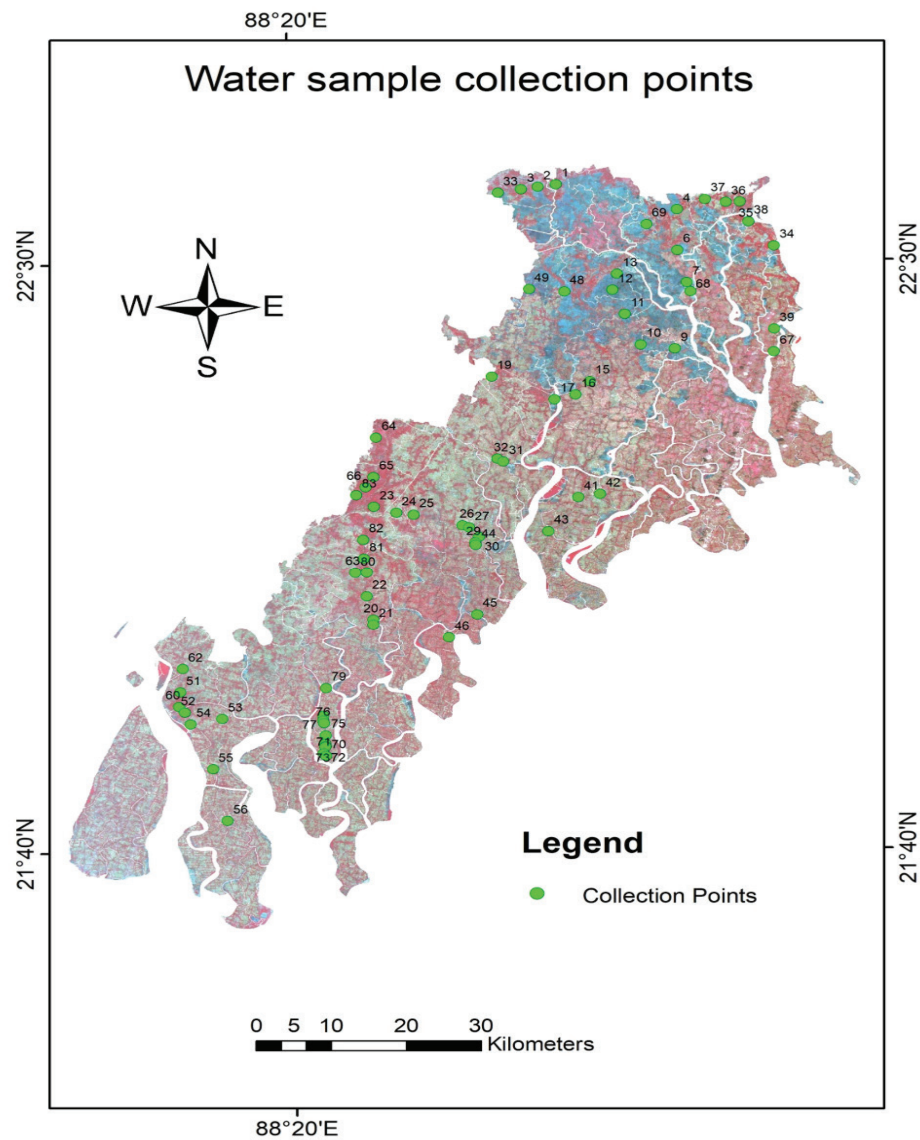

Fig. 4. *Pond water sample collected points*

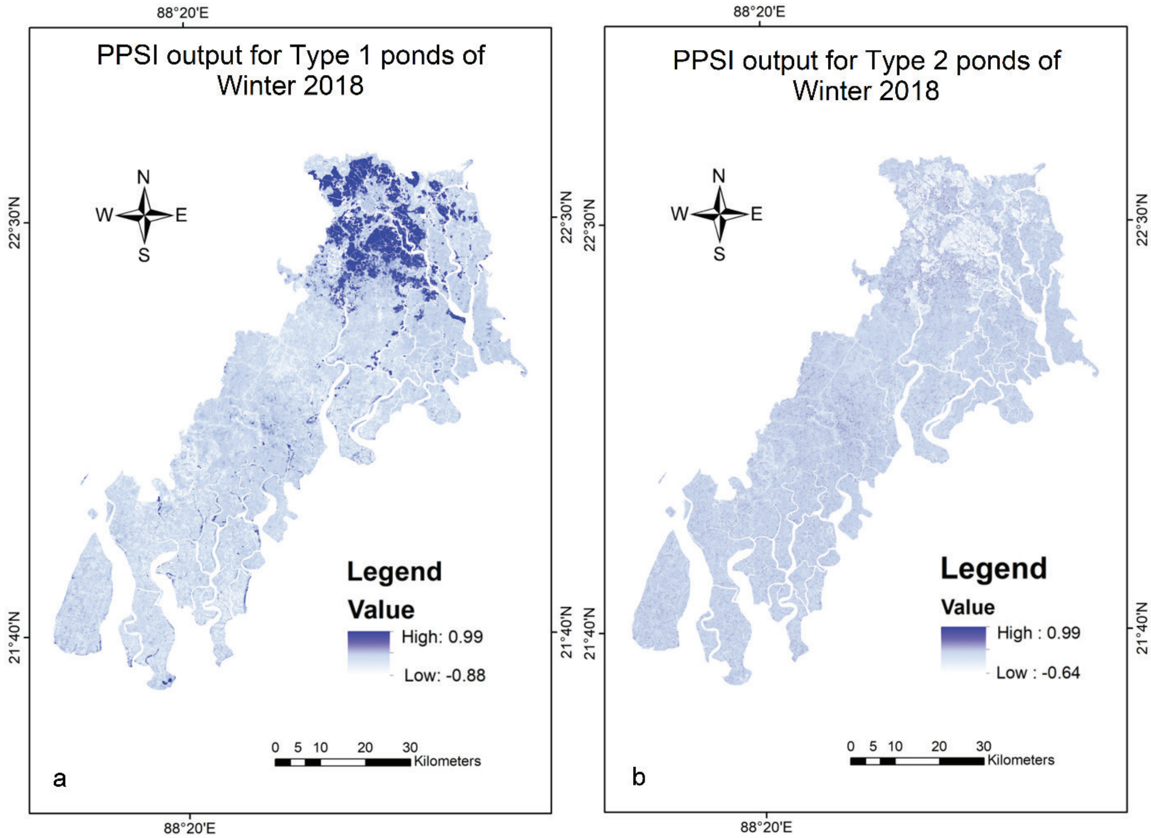

Fig. 5. *PPSI output of Type 1 ponds with typical reflectance of water and Type 2 ponds which were surrounded by vegetation and has a unique reflectance spectra*

A mask layer for extracting the ponds has been created from the decision tree output as shown in Fig. 6a. This layer was used to extract the water bodies from the winter 2019 dataset and subjected to accuracy assessment. The field data and also Google Earth were used to validate the extracted ponds and the overall accuracy of the pond delineation was found to be 91.45% with a kappa coefficient (κ) of 0.81 (Table 4). Hence, the decision tree which used PPSIs and NDVI resulted in delineating even small agricultural ponds in the study area with good accuracy.

Accuracy of turbidity indices

The pond water samples collected were tested at the Environmental Laboratory of the university. The statistical parameters of the results of 71 samples were given in Table 5. The output of the turbidity indices obtained was divided into three classes (Clear, turbid and highly turbid), with reference to the 35 samples from the total collected. The thresholds used over the turbidity indices have been tabulated (Table 6) and the remaining 36 samples were used for validating theindices.

The accuracy of the NDTI (Table 7) and SNDTI (Table 8) were tabulated below for comparison.The overall accuracy and kappa coefficient for NDTI are 69% and 0.37 respectively, meanwhile for SNDTI are 83% and 0.55 respectively. The consumer accuracy has been increased in SNDTI for clear and turbid classes. The accuracy (R^2) of using correlation of the ratio of red and green bands for turbidity retrievals was found to be 0.5469, 0.84 and 0.941 by Somvanshi *et al.* (2012),Quang *et al.* (2017) and Elhag *et al.* (2019), respectively. In our study, it has been found that SNDTI more accurately classified the ponds as clear, turbid and highly turbid than NDTI. Thus, a mathematical modification in NDTI worked well with this study dataset to differentiate between various turbidity classes.

So, the SNDTI was applied for the remaining five datasets of the different seasons to compare the turbid pond area, season-wise. Figs. 7, 8 and 9 show the turbidity classes in the seasons of post-monsoon,

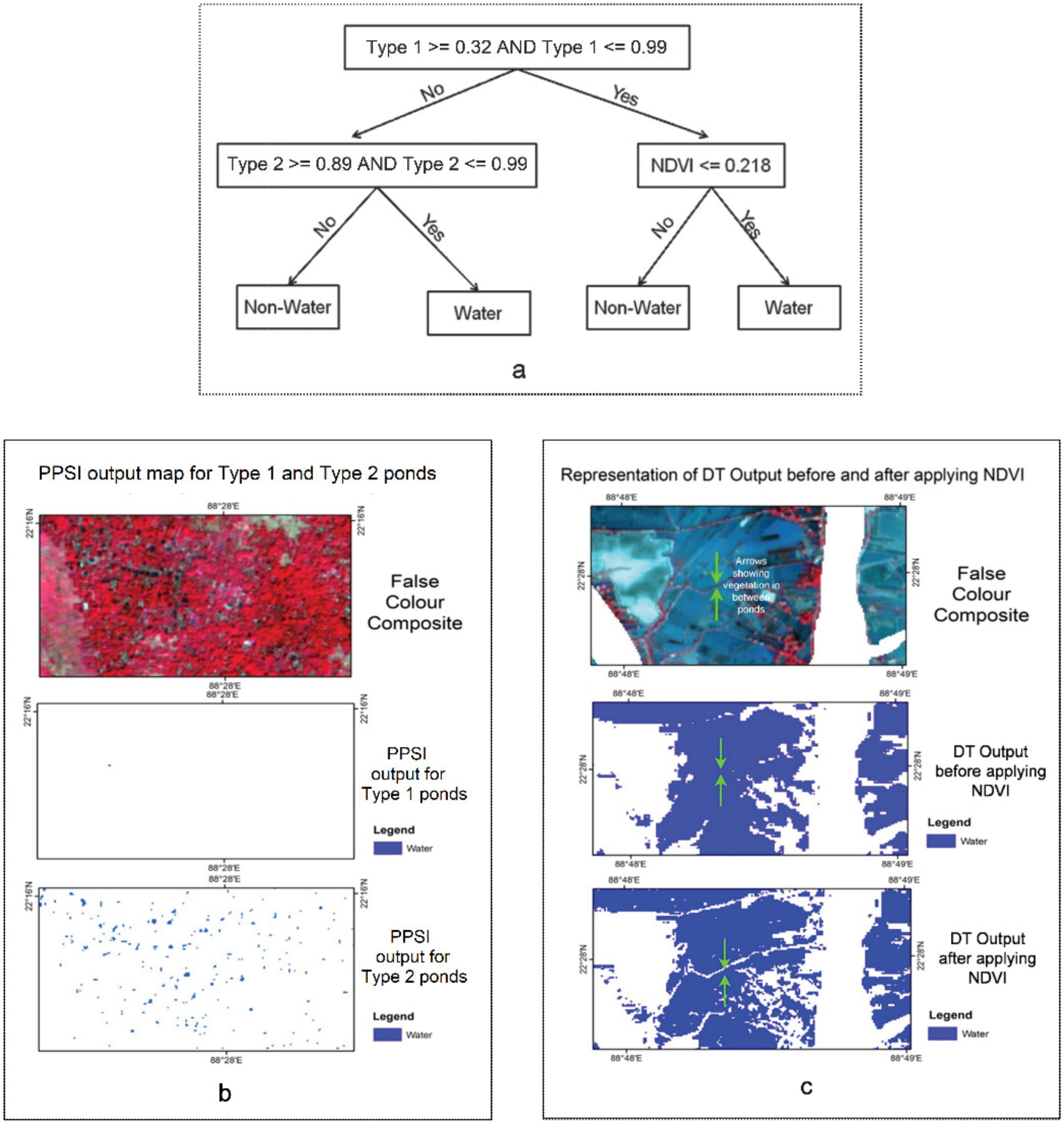

Fig. 6 (a). *Decision Tree (DT),* ***(b).*** *Justification of separating into Type 1 and Type 2 ponds,* ***(c).*** *Justification of using NDVI in DT*

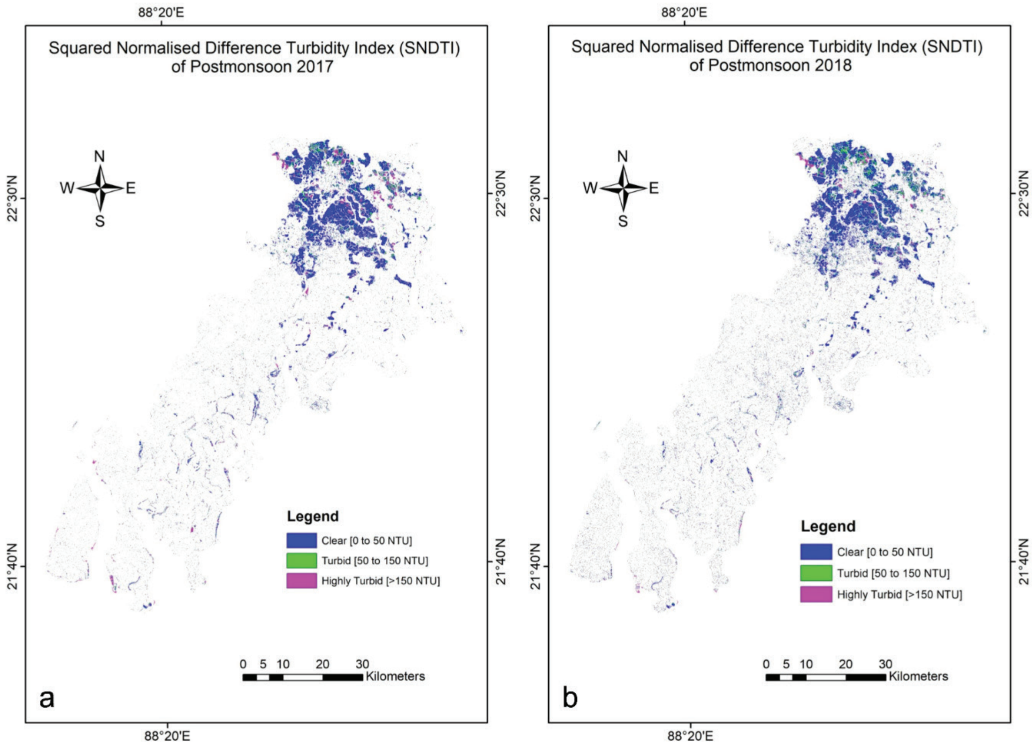

Fig. 7. *Turbidity variation obtained by SNDTI in post-monsoon seasons of (a) 2017 and (b) 2018*

summer and winter respectively. The two-year average, the total surface area of ponds estimated in the post-monsoon, summer and winter seasons were 513.56 km^2, 476.74 km^2 and 424.67 km^2, respectively. The area under different turbidity classes was calculated from the individual datasets and represented in Fig.10. The average areas of ponds detected under each of the 19 blocks for the three seasons are shown in Fig. 11.

Analysis of turbidity and salinity

The statistical variation of turbidity and salinity from the samples collected has been presented in the form ofa box-whiskers plot (Fig. 12) and the distribution of Type 1 ponds and Type 2 ponds over the turbidity and salinity classes have been studied (Table 9). The turbidity means of Type 1 and Type 2 ponds were 75.37 and 25.99 NTU, respectively. Irrespective of the types, turbidity values showed a wider range in comparison to the salinity values.

Many approaches have been used to relate turbidity and salinity values. The distribution of the ponds based on both salinity and turbidity has been given in Table 10. The test results showed that 42 ponds were fresh water and clear, highly turbid class showed more or less equal distribution of fresh water and saline ponds. The main inference is that most of the saline ponds (> 2ppm) i.e., 15 ponds out of 20 have been found to clear water ponds, ensuring that 75% of the saline ponds were clear.

Now, concerning the Type 1 and Type 2 ponds (Table 11), out of the 20 saline water samples, 19 belonged to Type 1 ponds and only one water sample (Sample no. 3 in Fig. 5 - top left) was from a Type 2 pond. The mentioned pond was found to be connected to a creek originating from one of the tidal rivers of the Sundarban delta. It is observed that all the saline ponds in the study area are Type 1 ponds (except the one connected to any creek), but vice-versa did not hold true, *i.e.*, all the Type 1 ponds were not saline. It enlightens the fact that the Type 2 ponds may have less depth and impounded with a cemented or stone flooring due to which there is no effect of salinity and, also from the field knowledge, Type 2 ponds are mainly the village ponds owned by several households. Whereas, Type 1 ponds are the lakes orbheries which are commonly found only with earthen flooring and embankment, due to which the saline ponds are prevalent in Type 1. As the 19 saline ponds do not have any connection to the tidal

Table 4. *Accuracy of delineation of ponds*

Classes	Error of omission (%)	Error of commission (%)	Producer accuracy (%)	Consumer accuracy (%)
Water	20.27	24.86	79.73	97.76
Non-water	1.15	1.03	98.85	88.53
Overall accuracy	91.45			
Kappa	0.813			

Table 5. *Statistical parameters for the parameters analysed from lab*

Statistical parameter	Turbidity (NTU)	Salinity (ppt)
Minimum	1.33	0.16
Maximum	570	21.25
Average	49.64	2.73
Standard deviation	93.89	4.16

NTU - Nephelometric Turbidity Unit; ppt - parts per trillion

Table 6. *Thresholds values used over output image*

Classes	Indices	
	NDTI	SNDTI
Clear	-1 to -0.6	-1 to -0.132
Turbid	-0.6 to -0.25	-0.132 to -0.0703
Highly turbid	-0.25 to 1	-0.0703 to 1

Table 7. *Confusion matrix and accuracy table of ground truth and NDTI*

	Classes	Clear	Turbid	Highly Turbid	Sum
Ground truth	Clear	20	5	4	29
	Turbid	1	3	0	4
	Highly turbid	0	1	2	3
	Sum	21	9	6	36

Classes	Error of ommision (%)	Error of commision (%)	Producer accuracy (%)	Consumer accuracy (%)
Clear	31.03	42.86	68.97	95.24
Turbid	25.00	11.11	75.00	33.33
Highly turbid	33.33	16.67	66.67	33.33
Overall accuracy	69.44			
Kappa	0.374			

Table 8. *Confusion matrix and accuracy table of ground truth and SNDTI*

	Classes	Clear	Turbid	Highly turbid	Sum
Ground truth	Clear	25	1	3	29
	Turbid	1	3	0	4
	Highly turbid	1	0	2	3
	Sum	27	4	5	36

Classes	Error of ommision (%)	Error of commision (%)	Producer accuracy (%)	Consumer accuracy (%)
Clear	13.79	14.81	86.21	92.59
Turbid	25.00	25.00	75.00	75.00
Highly turbid	33.33	20.00	66.67	40.00
Overall accuracy	83.33			
Kappa	0.552			

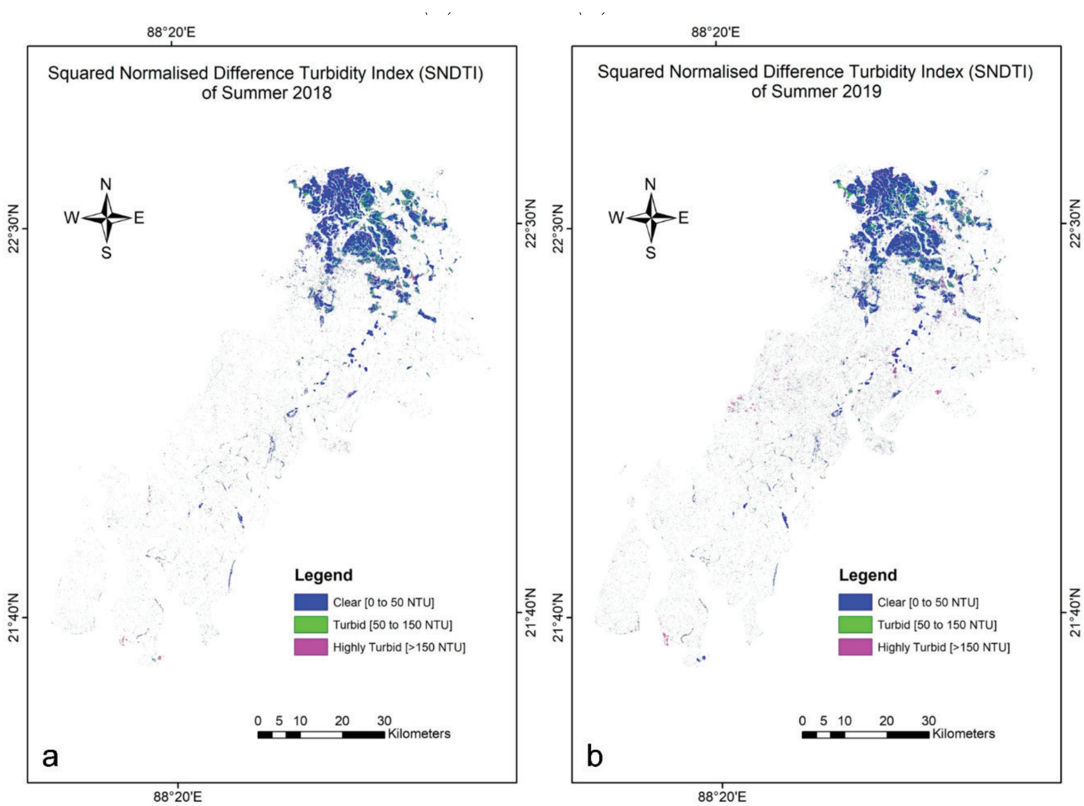

Fig. 8. *Turbidity variation obtained by SNDTI in summer season (a) 2018 and (b) 2019*

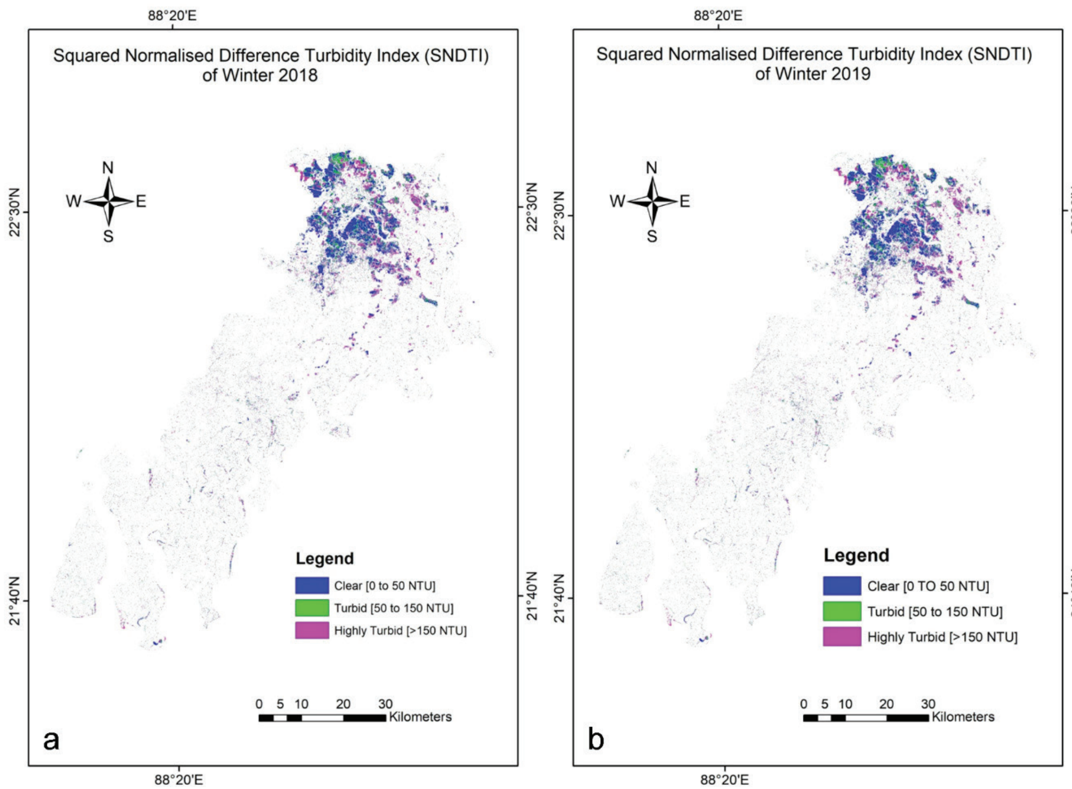

Fig. 9. *Turbidity variation obtained by SNDTI in winter season (a) 2018 and (b) 2019*

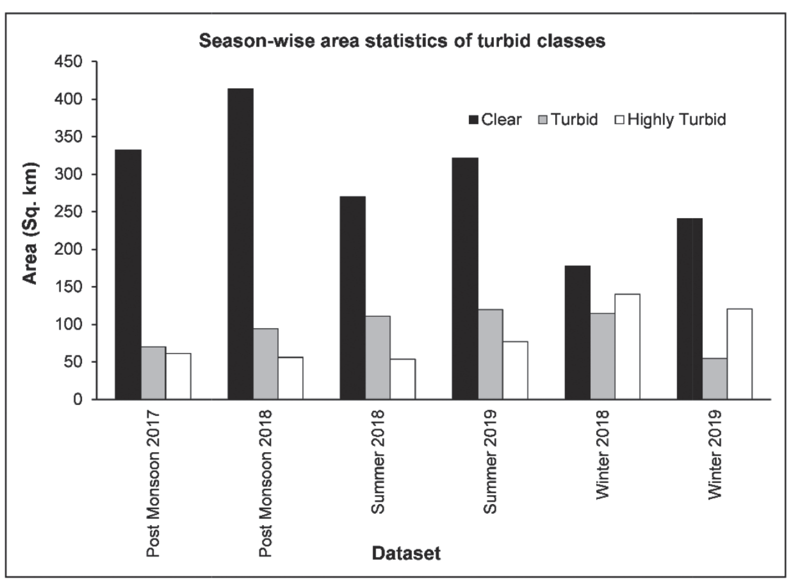

Fig. 10. *Area statistics of ponds in the study area*

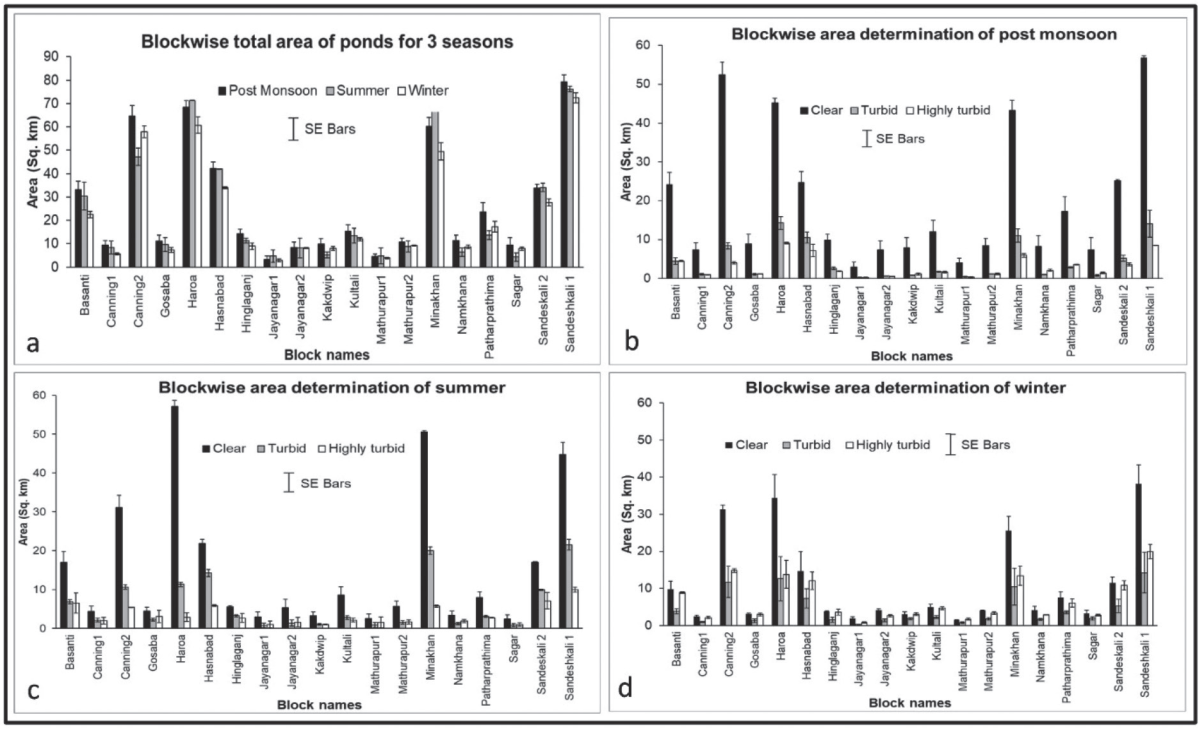

Fig. 11 (a). *Block wise area statistics of total ponds in the study area,* ***(b).*** *Block wise area statistics of post-monsoon season,* ***(c).*** *Block wise area statistics of summer season,* ***(d).*** *Block wise area statistics of winter season*

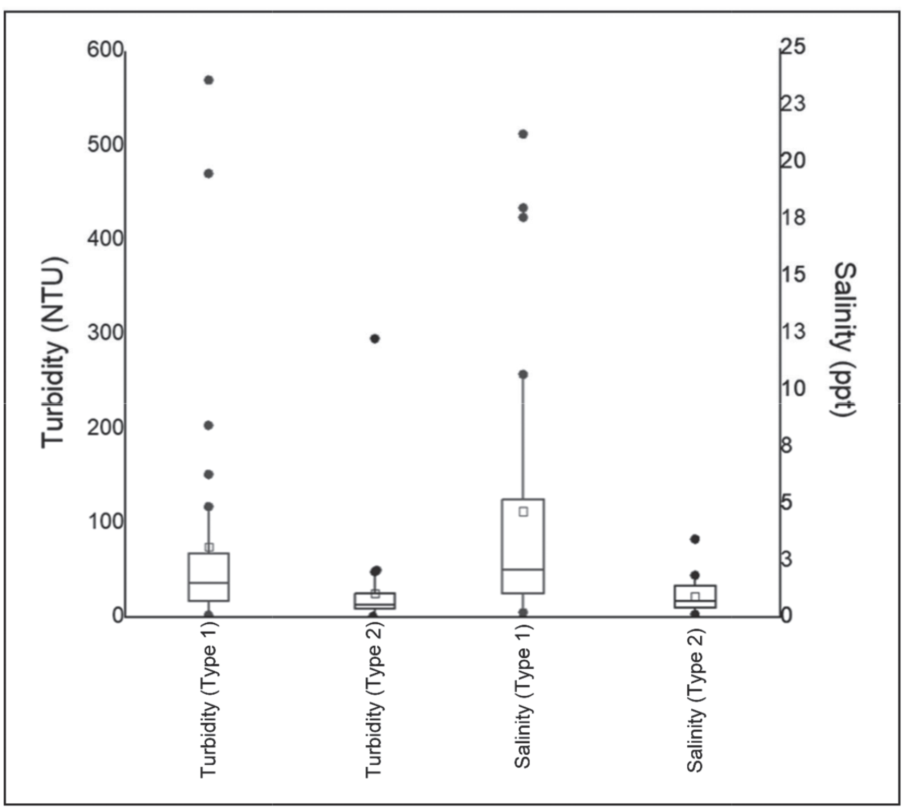

Fig. 12. *Box-whiskers plots of turbidity and salinity*

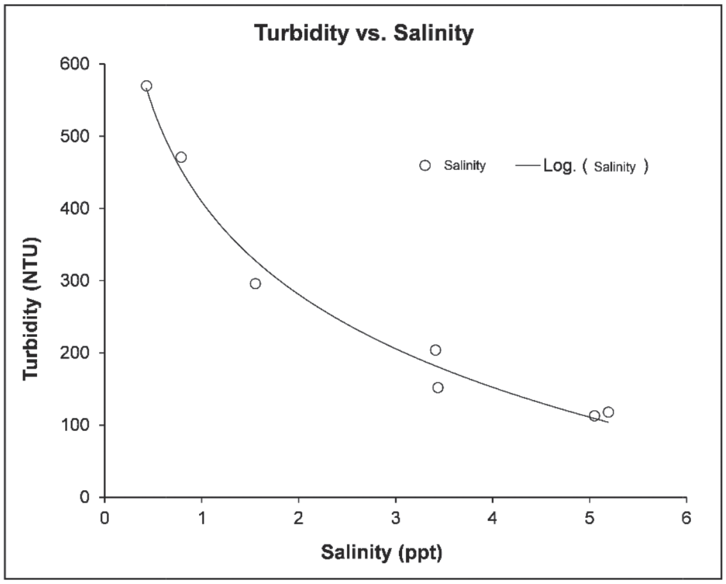

Fig. 13. *Correlation graph of turbidity and salinity*

Table 9. *Distribution of Type 1 and Type 2 ponds across different turbidity and salinity classes*

Ponds	Turbidity classes			Salinity classes	
	Clear	Turbid	Highly turbid	Fresh	Saline
Type 1	22	8	4	15	19
Type 2	35	1	1	36	1

Table 10. *Distribution of freshwater and saline ponds across different turbidity classes based on ground truth and SNDTI classified output*

Turbidity classes	Based on ground truth		Based on SNDTI classified output	
	Fresh	Saline	Fresh	Saline
Clear	42	15	40	13
Turbid	6	3	5	1
Highly turbid	3	2	6	6

Table 11. *Distribution of fresh water and saline ponds across different turbidity classes for Type 1 and Type 2 ponds*

Turbidity classes	Type 1 ponds		Type 2 ponds	
	Fresh	Saline	Fresh	Saline
Clear	8	14	34	1
Turbid	5	3	1	0
Highly turbid	2	2	1	0

creeks or rivers, the cause of the salinity can be due to the capillary rise of salt water. Any future studies aiming to delineate only the saline ponds can proceed only with the Type 1 ponds *i.e.,* the ponds with the typical spectral signature of water, as the salinity was not found in the Type 2 ponds.

The turbidity and salinity of the ponds were inversely proportional to each other. It is clear from the graph (Fig. 13) that salinity decreased with an increase in turbidity. This is because the salt ions collect suspended particles and bind them together, thereby increasing their weights and the likelihood of settling at the bottom of the ponds. Due to the same phenomenon, estuaries and oceans generally tend to have higher clarity and lower average turbidity than lakes and rivers (Li and Liu, 2019). In the present study, the above relationship was found in the water samples wherein turbidity was above 100 NTU.

A newly formed index, the Pond Probability Spectral Index (PPSI) along with NDVI used in the decision tree algorithm excelled in delineating even the small agricultural ponds in the study area with an overall accuracy of 91%. The new correlation index PPSI is suggested for further studies in the extraction of waterbodies and other features, provided their ‘pure spectra’ has been used as the reference spectrum. The total estimated pond area in the Sundarban region was 471.66 km^2 (average of three seasons estimations) and the highest average pond area was recorded in the Sandeshkhali-I block.

In classifying the turbid ponds, modified SNDTI (Overall accuracy = 83%) was found proficient than the conventionally used NDTI (Overall accuracy = 69%). Even though squaring of band values in the normalised indices gave a mathematically enhanced result and increased the accuracy in this case, further in-depth studies might be needed for its global usage over the other normalised indices. It is believed that this approach of turbidity characterisation if properly coordinated with *in-situ* monitoring will act as an early warning system to preserve aquatic life and to prevent the problems such as gastrointestinal and other bacterial diseases in humans.

The relationship between the salinity and turbidity of the ponds was found to be inversely proportional, only to the water having turbidity of more than 100 NTU. As many researchers explained that turbidity does not exist in highly saline water, it has been proved in the field conditions of Sundarbans, West Bengal. So, in this study, the objective of delineating the saline ponds from the satellite data by detecting the turbidity alone was not achieved. This study can be improved by taking some additional factors like groundwater quality, water table, lithological conditions, soil types, rainfall, etc., into consideration.

CONFLICTS OF INTEREST

There are no conflicts of interest.

REFERENCES

Al-Sameraiy, M. (2012). A novel water pre-treatment approach for turbidity removal using date seeds and pollen sheath. *Journal of Water Resource and Protection* **04**(02): 79-92. https://doi.org/10.4236/jwarp.2012.42010.

Asrafuzzaman, Md., Fakhruddin, A.N.M. and Hossain, Md. A. (2011). Reduction of turbidity of water using locally available natural coagulants. *ISRN Microbiology* **2011**: 632189. https://doi.org/10.5402/2011/632189.

Dörnhöfer, K., Göritz, A., Gege, P., Pflug, B. and Oppelt, N. (2016). Water constituents and water depth retrieval from Sentinel-2A - A first evaluation in an oligotrophic lake. *Remote Sensing* **8**(11). https://doi.org/10.3390/rs8110941.

Du, Y., Zhang, Y., Ling, F., Wang, Q., Li, W. and Li, X. (2016). Water bodies mapping from Sentinel-2 imagery with modified normalized difference water index at 10-m spatial resolution produced by sharpening the SWIR band. *Remote Sensing* **8**(4). https://doi.org/10.3390/rs8040354.

Elhag, M., Gitas, I., Othman, A., Bahrawi, J. and Gikas, P. (2019). Assessment of water quality parameters using temporal remote sensing spectral reflectance in arid environments, Saudi Arabia. *Water (Switzerland)* **11**(3). https://doi.org/10.3390/w11030556.

Ghosh, A. (2017). *Sustainability Conflicts in Coastal India: Hazards, Changing Climate and Development Discourses in the Sundarbans,* Springer Cham. 245 p. https://doi.

org/10.1007/978-3-319-63892-8.

Hendges, E.R., Fallador, F.A.C. and Andres, J. (2018). Correlation study between land use and covering with surface temperature registered by Landsat 8 satellite. *Sociedade & Natureza* **32**: 338-347.

Jawak, S.D., Kulkarni, K. and Luis, A.J. (2015). A review on extraction of lakes from remotely sensed optical satellite data with a special focus on cryospheric lakes. *Advances in Remote Sensing* **04**(03): 196-213. https://doi.org/10.4236/ars.2015.43016.

Krishan, G., Sudarsan, N., Sidhu, B. S. and Vashisth, R. (2021). Impact of lockdown due to COVID-19 pandemic on groundwater salinity in Punjab, India: Some hydrogeoethics issues. *Sustainable Water Resources Management* **7**:27. https://doi.org/10.1007/s40899-021-00510-2.

Kumar, T., Mandal, A., Dutta, D., Nagaraja, R.and Dadhwal, V.K. (2017). Discrimination and classification of mangrove forests using EO-1 Hyperion data: A case study of Indian Sundarbans. *Geocarto International* **34**(4): 415-442. https://doi.org/10.1080/10106049.2017.1408699.

Kutser, T., Paavel, B., Verpoorter, C., Ligi, M., Soomets, T., Toming, K. and Casal, G. (2016). Remote sensing of black lakes and using 810 nm reflectance peak for retrieving water quality parameters of optically complex waters. *Remote Sensing* **8**(6). https://doi.org/10.3390/rs8060497.

Lacaux, J.P., Tourre, Y.M., Vignolles, C., Ndione, J.A. and Lafaye, M. (2007). Classification of ponds from high-spatial resolution remote sensing: Application to Rift Valley fever epidemics in Senegal. *Remote Sensing of Environment* **106**(1): 66-74. https://doi.org/10.1016/j.rse.2006.07.012.

Li, D. and Liu, S. (2019). Sensors in water quality monitoring. In: *Water Quality Monitoring and Management,* D. Li and S. Liu (eds.), Academic Press, USA. 361 p. https://doi.org/10.1016/b978-0-12-811330-1.00001-6.

Li-Gang, F., Shui-Sen, C., Li, H. L. and Cai-Dong, G. (2008). Monitoring water constituents and salinity variations of saltwater using EO-1 Hyperion satellite imagery in the Pearl river estuary, China. *International Geoscience and Remote Sensing Symposium* **1**(1): 438-441. https://doi.org/10.1109/IGARSS.2008.4778889.

Martins, V.S., Barbosa, C.C.F., de Carvalho, L.A.S., Jorge, D.S.F., Lobo, F. de L. and de Moraes Novo, E.M.L. (2017). Assessment of atmospheric correction methods for Sentinel-2 MSI images applied to Amazon floodplain lakes. *Remote Sensing* **9**(4). https://doi.org/10.3390/rs9040322.

Mukherjee, S. (2014). Studies on removal of organic and inorganic load from wastewater using coagulation-flocculation and advanced techniques. *Unpublished Ph.D. Thesis,* Maulana Abdul Kalam Azad University of Technology, West Bengal, India.

Müller, D.N., Wilck, N., Haase, S., Kleinewietfeld, M. and Linker, R.A. (2019). Sodium in the microenvironment regulates immune responses and tissue homeostasis. *Nature Reviews Immunology* **19**(4): 243-254. https://doi.org/10.1038/s41577-018-0113-4.

Palmer, S.C.J., Kutser, T. and Hunter, P.D. (2015). Remote sensing of inland waters: Challenges, progress and future directions. *Remote Sensing of Environment* **157**: 1-8. https://doi.org/10.1016/j.rse.2014.09.021.

Petus, C., Chust, G., Gohin, F., Doxaran, D., Froidefond, J.-M. and Sagarminaga, Y. (2010). Estimating turbidity and total suspended matter in the Adour River plume (South Bay of Biscay) using MODIS 250-m imagery. *Continental Shelf Research* **30**(5): 379-392.

Quang, N.H., Sasaki, J., Higa, H. and Huan, N.H. (2017). Spatiotemporal variation of turbidity based on Landsat 8 OLI in Cam Ranh Bay and Thuy Trieu Lagoon, Vietnam. *Water (Switzerland)* **9**(8). https://doi.org/10.3390/w9080570.

Rana, H. and Neeru, N. (2017). Hybrid technique for detection of water using satellite images. *International Journal of Advanced Research in Computer Science* **8**(7): 659-666. https://doi.org/10.26483/ijarcs.v8i7.4361.

Rusydi, A.F. (2018). Correlation between conductivity and total dissolved solid in various type of water: A review. IOP Conference Series: *Earth and Environmental Science* **118**:012019. https://doi.org/10.1088/1755-1315/118/1/012019.

Sarp, G. and Ozcelik, M. (2017). Water body extraction and change detection using time series: A case study of Lake Burdur, Turkey. *Journal of Taibah University for Science* **11**(3): 381-391. https://doi.org/10.1016/j.jtusci.2016.04.005.

Shah, D. and Zaveri, T. (2021). Hyperspectral endmember extraction using Pearson's correlation coefficient. *International Journal of Computational Science and Engineering* **24**(1): 89-97. https://doi.org/10.1504/IJCSE.2021.1136 6.

Somvanshi, S., Kunwar, P., Singh, N.B., Shukla, S.P. and Pathak, V. (2012). Integrated remote sensing and GIS approach for water quality analysis of Gomti river, Uttar Pradesh. *International Journal of Environmental Sciences* **3**(1): 62-75. https://doi.org/10.6088/ijes.2012030131008.

Toming, K., Kutser, T., Laas, A., Sepp, M., Paavel, B. and Nõges, T. (2016). First experiences in mapping lake water quality parameters with Sentinel-2 MSI imagery. *Remote Sensing* **8**(8): 1-14. https://doi.org/10.3390/rs8080640.

Zhang, C., Kovacs, J.M., Liu, Y., Flores-Verdugo, F. and Flores-de-Santiago, F. (2014). Separating mangrove species and conditions using laboratory hyperspectral data: A case study of a degraded mangrove forest of the Mexican Pacific. *Remote Sensing* **6**(12): 11673-11688. https://doi.org/10.3390/rs61211673.